

## SuperRez-II adaptive multispectral fundus imager

A.V. Larichev<sup>a</sup>, J.J. Otten<sup>b</sup>, N.G. Irochnikov<sup>a</sup>, P. Soliz<sup>c</sup>, G.R.G. Erry<sup>d</sup>, V.Y. Panchenko<sup>a,c</sup>.

<sup>a</sup>M.V.Lomonosov Moscow State Univ., Moscow, Russia, <sup>b</sup>Photon Research Associates, <sup>c</sup>Orion International technologies, <sup>d</sup>VisionQuest Biomedical, Albuquerque NM, <sup>e</sup>Institute on Laser and Information Technologies, Shatura, Moscow Region, Russia.

### ABSTRACT

A new significantly redesigned version of clinically applicable adaptive optics multispectral fundus imager is presented. Along with greatly improved adaptive system loop rate, the device performs reliably and is convenient for use in clinical practice. This new imager has allowed us to use new approaches for retina image analysis and obtain original results on the distribution of aberrations in the human eye.

Keywords: Adaptive optics, eye aberrations, wavefront sensor, modal wavefront corrector.

### 1.INTRODUCTION

A standard, commercially available fundus imager is limited by the imperfect optics of the eye to a spatial resolution of 20 $\mu$ m under optimal conditions. There are many cases when a better resolution is desired, for example in the detection of signs of age related macula degeneration, diabetic retinopathy and other retinal diseases. Adaptive optics has been shown to compensate for the aberrations in the eye<sup>1,2</sup>. If all the aberrations were corrected, then only the size of the eye's pupil would be the limit of the system resolution. From the Rayleigh criterion the diffraction limit of 3  $\mu$ m can be achieved for 8 mm dilated pupil.

Standard adaptive optics systems, because of their complexity and expense are not realistic candidates for a clinical environment. Lower cost and for a clinically friendly system was our objective. Our previous fundus imager, SuperRez-I<sup>3,4</sup>, was integrated into a KFG-2 model, produced by Zagorsk Optics and Mechanics Plant joint-stock company (AO ZOMZ). The SuperRez imager combines the Shack-Hartmann wavefront sensor for measuring aberrations in the eye, a flexible mirror for their correction, a multispectral illuminating unit and a high resolution CCD camera for picture acquisition. The adaptive optics part of the system can compensate up to fifth order aberrations. However, the close loop rate of the system was not sufficient for the fast fluctuating aberrations of a human eye, so some redesign and improvement of the system were necessary.

The new system SuperRez-II, based on the 77-Hz DALSA camera is able to compensate for aberrations of the eye in a real-time. This allows one to obtain images of the retina with a greater resolution. Now, the limiting factor for resolution is the anisoplanatism in the human eye, which according to<sup>5</sup> the isoplanatic region of the eye is about 4° and can be enhanced by some technical means, described below, up to 5°. This angle is just a small portion of the 15°-field of view of the fundus imager. In order to address this problem, we studied distribution of the aberrations in the eye from a model approach, and by obtaining them from the image of retina using technique, previously described in<sup>6</sup>.

### 2.EXPERIMENTAL SETUP

The first version of our adaptive multispectral fundus imager has been previously described<sup>3</sup>. In this paper we show a modern version, SuperRez-II, emphasizing its distinguishing features.

A schematic of the SuperRes-II is shown in Fig. 1. Optical elements belonging to this device are circumscribed on the scheme by the dotted line. The standard KFG-2 fundus camera is supplemented with an adaptive unit, allowing the compensation of eye aberrations and retina imaging by means of a high-resolution digital camera.

The series model of KFG-2 underwent a number of modifications. To improve the diffraction-limited resolution of the system to 200 lines per mm (the resolution value is determined at the half-maximum of the modulation transfer function), the diameter of the entrance pupil of this device was extended from 2 to 4.8 mm. The illuminating halogen lamp and pulsed xenon lamp with the corresponding collecting optics, as well as power supplies of these lamps, were removed. The observation binocular, employed for pointing of the fundus camera at the human eye, was replaced by an IR guidance system including the lens (17) and the IR CCD camera (18).

To illuminate the retina for both the guidance and the digital photo-registration regimes, an illuminator (24) was fabricated. A 300-W xenon lamp with a small arc gap was used as a light source. Emission of the lamp was



patient's eye, to the optical path.

The illuminating radiation, propagating in the fiberglass bundle, passed through the annular diaphragm (22). The objective (*Ob3*) imaged this diaphragm on the deflecting annular mirror (19), which was used to separate the illuminating beams, propagating in forward and backward directions, from each other. The main objective (*Ob1*) of the camera imaged the annular light source on the eye cornea (20), with the central part of the cornea remaining unlit. The entrance pupil of the device was located entirely inside the unlit area. This provided an additional selection of corneal flares. Thus, spurious reflections did not appear in the area of the entrance pupil, and did not cause the artifacts in the retinal image. This illumination system also provided the uniform lighting of the eye fundus. A more detailed description of operation principles of such ophthalmologic devices can be found in other papers<sup>7,8</sup>.

The radiation reflected by the retina emerged from the eye as a quasi-parallel beam. The eye-pupil image was constructed in the plane of the annular mirror (19) by the objective *Ob1* and *Ob2* of the camera. The beam diameter corresponded to the central aperture of the annular mirror. Next, radiation propagated through the objective (*Ob2*), fixed to the device, providing the transverse displacement and allowing the compensation of the eye ametropia within the range from -20 to +20 D.

After passing through the optical elements of the fundus camera, the light was incident on the spectral beamsplitter (16). A part of emission, corresponding to the IR emission (800-1000 nm) of the halogen lamp, was deflected by the beamsplitter to the guidance system. The lens (17) formed the retinal image in the plane of the IR video camera (18). The image registered by the video camera was displayed by the computer monitor and was used for the focusing of the fundus camera to the selected area of the retina.

Light, having passed through beamsplitters (16) and (15), was incident on the adaptive mirror (14). We used a modal bimorph corrector, which was similar to that described in paper<sup>9</sup>. 24 electrodes of the mirror made it possible to compensate for aberrations of up to the fifth order inclusive. The surface of the mirror was conjugate to the plane of the eye pupil and to the entrance pupil of the fundus camera.

The beam reflected by the deformable mirror was incident on the beamsplitter (11), transmitting the visible 440-670-nm light and reflecting the 680-800-nm radiation. The transmitted radiation passed through the lens (12), which formed the eye-fundus image on the matrix of the KRC4096 digital video camera. One pixel of this camera corresponded to the retina region of size 2- $\mu$ m. The photosensitive matrix had the resolution of 4096 x 4096 pixels. The signal of the matrix was digitized by means of the 14-bit ADC. For typical levels of the retina illumination, the camera provided the signal-to-noise ratio of 56 dB (shot noise limited). The data transmission rate to the computer, provided by the digital interface, was one frame per second.

The configuration of the wavefront sensor is in many respects similar to the device described in a previous paper<sup>10</sup>. The 780-nm radiation of the IR diode laser was used to form a reference light source on the retina. IR radiation of this range has the high coefficient of reflection from the eye fundus (10 % -12 %)<sup>11</sup>, and is more comfortable to a human eye than visible light. Moreover, having chosen such a wavelength of the reference source, we separated the channel of the forming of the visible-light image of the retina from the aberration-measuring channel using the coherent IR radiation, by selecting the spectral characteristics of optical elements of the system.

Preliminarily, the laser beam (5) passed through the diaphragm (not shown in Fig. 1) of diameter 0.8 mm. The reduction of the beam diameter provided the conditions of single-pass measurements<sup>12</sup>. The power of radiation incident on the eye was 50  $\mu$ W, which was significantly lower than the maximum permissible power<sup>13,14</sup>. Then, the beam reflected from the inner face of the polarization cube (6), propagated through lenses (7) and (10), reflected from the adaptive mirror (14), and was directed into the optical channel of the fundus camera. After passing through the objectives (*Obj2*) and (*Obj1*), the laser radiation was focused by the eye elements onto the retina, forming the reference source. The radiation scattered by the retina was brought back to the system, and was directed to the Shack-Hartmann wavefront sensor after the reflection from the adaptive mirror (14). The lens raster of the sensor (2) was placed in the plane, which was optically conjugated to the plane of the eye pupil. Each lens (subaperture) of the raster had a 0.25-mm diameter and a 5-mm focal length. For the pupil diameter equal to 4.8 mm, radiation emerging from the eye illuminated about 120 subapertures of the raster. The wavefront under study was divided by the lenses of the sensor thus forming an array of spots (Hartmannogram) in the focal plane. Each spot of the Hartmannogram was an image of the reference source on the retina. The Hartmannogram was recorded by a CCD camera (1), located in the focal plane of the lens raster, and then was stored in the computer memory with the rate of 77 frames per second (30 fps in old version) and the resolution of 512x512 pixels.

The wavefront was reconstructed from measured local wavefront slopes by the method of least squares<sup>15</sup> as an expansion in up to 35 Zernike polynomials<sup>16</sup> and in response functions of the adaptive mirror. The time of processing of a Hartmannogram was 5 ms. Thus, the maximum speed of aberration measurement was limited by the video camera parameters (77-Hz frame rate).

The speckle field, resulting from scattering of the coherent laser radiation by the retina, lowers the quality of the Shack - Hartmann sensor signal and increases the error of the aberration measurement<sup>10</sup>. To suppress speckles in our system, we used the method of scanning of the reference-source position on the retina. For this purpose, the wedge with a small bias ( $1.0^\circ$ ) (8) was attached to the electric-motor axis. The rotation of the wedge caused the displacement of the reference source on the retina, resulting in a change in the speckle structure. For the electric-motor rotation speed of 50 rps, the characteristic time of a change in the speckle structure (0.2 ms) was much shorter than the integration time of the CCD camera (1) (12 ms), and, therefore, speckles were efficiently suppressed.

Because the laser radiation was twice (in a forward and backward passage) transmitted through a scanning wedge, the displacement of the reference source on the retina did not cause any displacement of the Hartmannogram spots. This is explained by the fact that the eye mainly works as a retro reflector, i. e., radiation scattered by the retina emerges from the eye at an angle equal to the angle of radiation incidence. Because the surface of the scanner mirror was optically conjugated to the entrance pupil of the system and the lens raster of the sensor, wavefront slopes caused by this mirror were compensated during the backward passage.

The response functions of the modal bimorph corrector are not completely orthogonal. This fact complicates the sensor controlling procedure. To orthogonalise the response functions, the electrodes were combined into 11 groups. The control voltage was simultaneously applied with different weights to all the electrodes in a group. The weights were experimentally determined from the condition that the response functions should be maximally close to Zernike functions. In most cases, the residual error of compensation of real-eye aberrations was less than 0.1-0.15  $\mu\text{m}$ . When the correction error reached this value, a computer automatically produced a synchronizing signal for the illuminator, and the eye fundus was photographed.

Note that the scanning technique, applied in phase distortion measurements, has an important feature, which does not concern speckle suppression. The human eye, as the most of optical systems, is not isoplanar<sup>17</sup>. This means that the measured phase distortions depend on the angular position of the reference source. In this case, it is impossible to determine aberrations in the entire field of view of the system by using a single reference source<sup>18</sup>. Therefore, the adaptive compensation improves the image quality only within the isoplanatism region. In some cases, it is preferable to correct for average aberrations in a large field of view and to improve the image quality within the large area, than to achieve a high resolution within the small area.

The scanning technique, as distinct from other methods, gives an opportunity to determine average aberrations by using only one reference source. Thus, while laser spot moves sufficiently fast, the phase distortions are being averaged over the scanning area. The size of this area can be varied by changing the mirror tilt angle. It is estimated in<sup>5</sup> that the isoplanatic region of the human eye is about  $4^\circ$ , so the usage of such a wedge widens the region in  $1^\circ$ , or in 20%.

The human-eye retina reflects a small part of the incident light<sup>11</sup>. In the experiment, the power of infrared radiation emerging from the eye did not exceed 25  $\mu\text{W}$ . Although all lenses were covered with antireflection coatings, the intensity of light reflected from lenses was comparable with that of useful signal. To suppress spurious reflections, the polarization cube (6) was set in such a way as to transmit the depolarized radiation scattered by the retina and to reflect polarized radiation scattered from optical surfaces. A diaphragm (not shown in Fig. 1), which also partially suppressed defocused reflections, was placed in the focal plane between lenses (3) and (4).

One of new features, introduced in SuperRez-II is the built-in reference source for the wavefront sensor calibration (Not shown on the Fig.1). This reference source allows the operator to easily recalibrate the system (after, for example, transportation, re-alignment etc.). It consists of an IR laser diode and precisely calibrated telescope, which produces a flat reference wavefront with absolute precision  $\lambda/10$ .

### 3.PERFORMANCE MEASUREMENTS

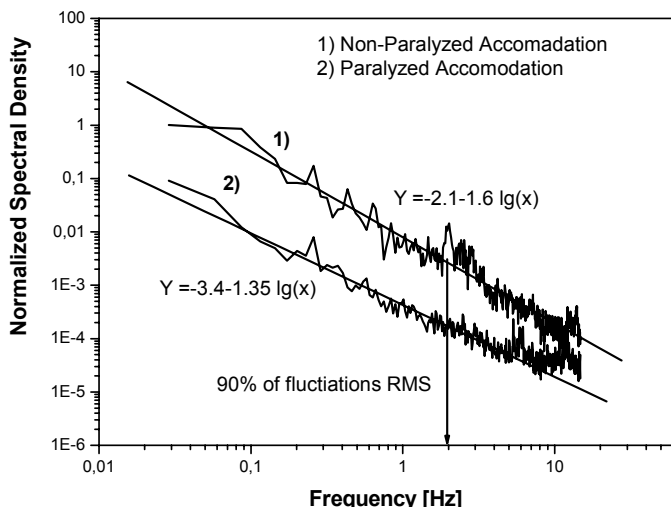


Figure 2. Temporal fluctuations of human eye aberrations. 4 subject averaged.

Our preliminary studies of the dynamics of human eye aberrations<sup>4</sup> show that 90% of integral spectral density of temporal fluctuations of the aberrations is below 2 Hz (See Fig.2). Therefore, the response time of an adaptive system capable of effectively compensating aberrations of the eye must be less than 0.5 s. Fig. 3 illustrates the comparison of response speed of SuperRez-I and SuperRez-II. The former, with the 30Hz-loop rate showed 1.5 s response time, which was too large for effective compensation of the eye aberrations in a real-time. The new one, the SuperRez-II demonstrates 5 times better result, which is good enough for the real-time compensation. To achieve this we have not only changed the previous 30-Hz camera for new 77-Hz, but also improved the adaptive mirror control algorithm, taking into account the timing characteristics of the system. The main feature of the new control algorithm is PID controller with dead time compensation. Due to upgrades in the wavefront sensor mathematics, the aberration measurements became more stable and reliable (that is obvious from Fig.3, compare the noise level), which in turn also improved adaptive

system performance.

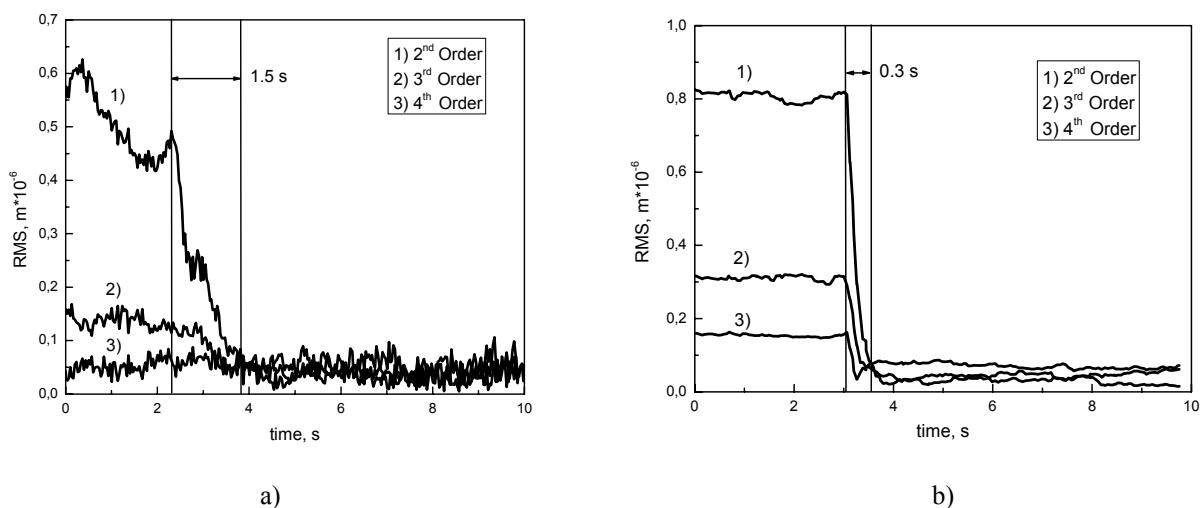


Figure 3. Aberration compensation in SuperRez-II vs. SuperRez-I: a) SuperRez-I with loop rate 30Hz; b) SuperRez-II with loop rate 77 Hz.

#### 4. ANGULAR ANISOPLANATISM OF THE HUMAN EYE

Adaptive optical system, using in the SuperRez-II is capable of measuring and compensating aberrations in a small angular region, determined by the system design and which is not larger than  $1^\circ$ . The isoplanatic region of the human eye is about  $4^\circ$  that results in  $5^\circ$  total angular diapason of aberration corrected field of view. Meanwhile, the fundus imager field of view is  $15^\circ$ . Our goal was to get information on the aberrations outside the isoplanatic region, in order to improve the resolution over the entire image.

First of all we made some theoretical estimations of aberration distribution of the human eye. Using Gullstrand model of the eye, we calculated how the magnitudes of several aberrations depend on the angle (See Fig.4).

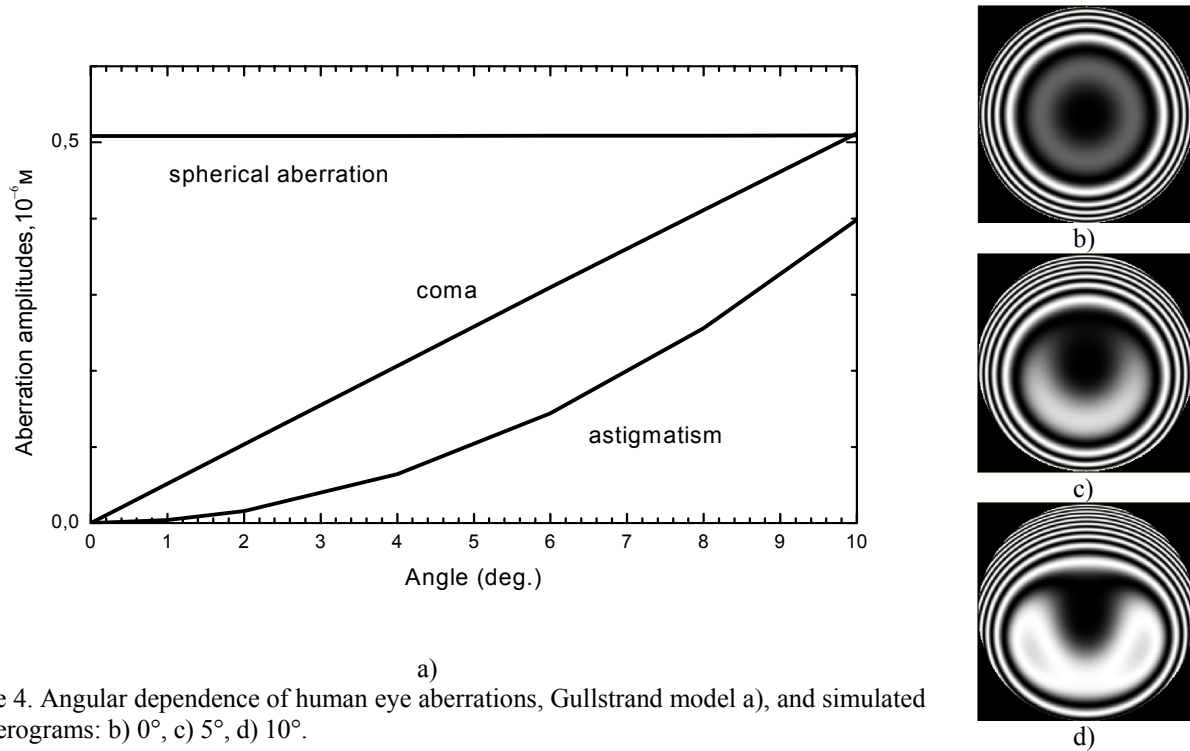


Figure 4. Angular dependence of human eye aberrations, Gullstrand model a), and simulated interferograms: b)  $0^\circ$ , c)  $5^\circ$ , d)  $10^\circ$ .

To obtain experimental data on the aberrations, we use the following approach: at first, we reconstruct the optical transfer function (OTF) according to the self-deconvolving data reconstruction algorithm (SeDDaRA), described in<sup>19</sup>. Then we find Zernike polynomial amplitudes, which fit the OTF using a pyramidal recursive algorithm<sup>6</sup>. If the nondisturbed image is  $f(x,y)$ , OTF is  $h(x,y)$ , and the image taken by the system is  $g(x,y)$ , then in the Fourier space  $(u,v)$ :

$$G(u, v) = F(u, v) \cdot H(u, v) + N(u, v), \quad (1)$$

where  $G, F, H$  are the Fourier spectra of  $g, f$  and  $h$  correspondingly,  $N$  is the noise spectrum. According to the original SeDDaRA algorithm  $H$  can be estimated as:

$$H(u, v) = \left[ K_G \cdot S \left\{ G(u, v) - N(u, v) \right\} \right]^{\alpha(u, v)}, \quad (2)$$

where  $K_G$  is the real positive scalar chosen to ensure that  $|H| \leq 1$ ,  $S$  is the smoothing operator and  $\alpha(u, v)$  is a tuning parameter. In<sup>19</sup> it is shown that although the best results require detailed knowledge of an averaged spectrum of nondisturbed image, rather good result can be achieved if  $\alpha$  is chosen as a some function of angular coordinates. In our case, we used

$$\alpha(u, v) = \left( 1 - e^{-\frac{u^2 + v^2}{2 \cdot r_a^2}} \right) \cdot a_{\max}, \quad (3)$$

where  $r_a$  and  $a_{\max}$  can be found as an approximation of a spectrum of a rather good image. Such a function is chosen to leave low spatial frequency harmonics intact, and to augment the higher frequency harmonics, that must restore the

initial image. Advantages of such an approach over iterative methods of blind deconvolution are the fastness of calculations and effectiveness of image restoration. Fig. 5 shows an example of the use of SeDDaRA algorithm on the retina images.

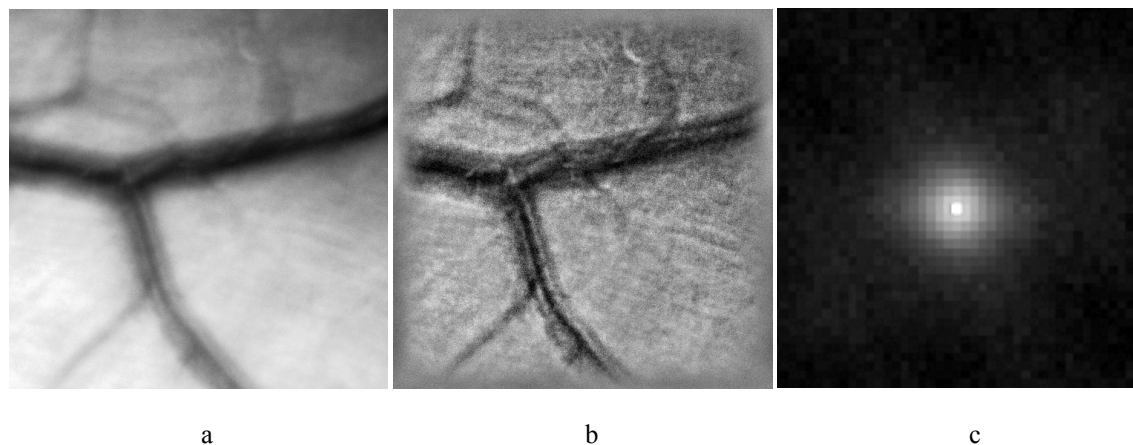


Figure 5. Initial a) , deconvolved by the use of SeDDaRA algorithm b) images and the PSF c).

The OTF, found from (2), was then approximated by an OTF calculated from the following equation:

$$\tilde{H}(u, v, \vec{a}) = \hat{F} \left\{ m(x, y) \cdot e^{-\frac{2\pi i \cdot \omega(x, y, \vec{a})}{\lambda}} \right\}, \quad (4)$$

where  $\vec{a} = \{a_0, a_1, a_2, \dots, a_N\}$  is a set of Zernike coefficient amplitudes,  $\hat{F}$  is a Fourier transformation, and

$$\omega(x, y, \vec{a}) = \sum_k a_k \cdot Z_k(x, y) \quad (5)$$

is the wavefront aberrations, expanded onto Zernike polynomials  $Z_k$ ,  $m(x, y)$  is the pupil function,  $\lambda$  is the wavelength. We used a pyramidal approach<sup>6</sup> and Nelder-Mead<sup>20</sup> algorithm for minimization of the error function

$$E(\vec{a}) = \sqrt{\sum_{u,v} (\tilde{H}(u, v, \vec{a}) - H(u, v))^2}. \quad (6)$$

This algorithm showed good convergence in most cases (see Fig. 6a).

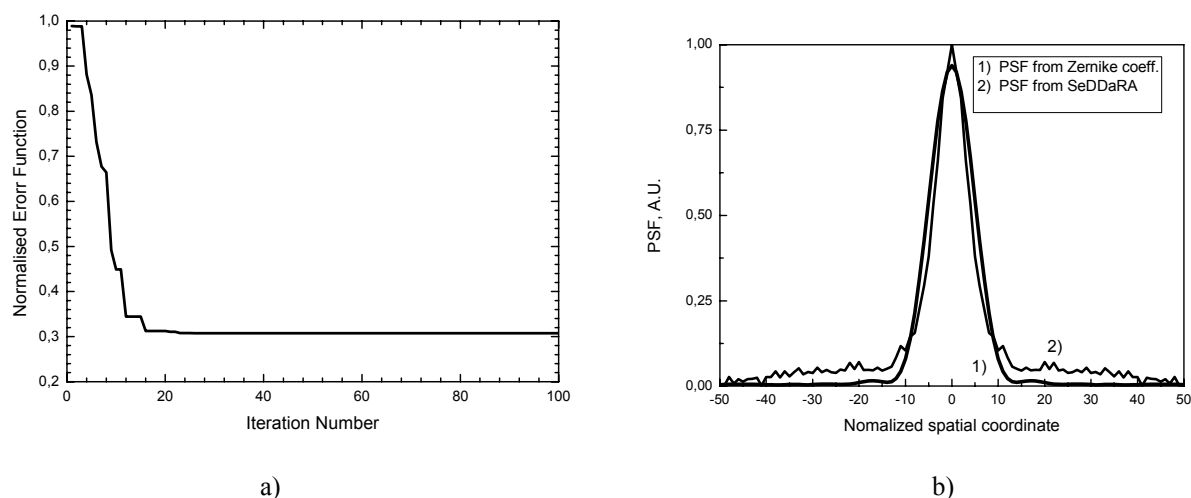


Figure 6. Pyramidal algorithm convergence a), PSFs found from SeDDaRA deconvolution and pyramidal approximation algorithms.

Figure 7. shows dependencies of defocus and astigmatism magnitudes on the angular position over the central part of the eye. We selected up to 9 regions on the retina, each of them contained sharp details like blood vessels on the Fig.5 in

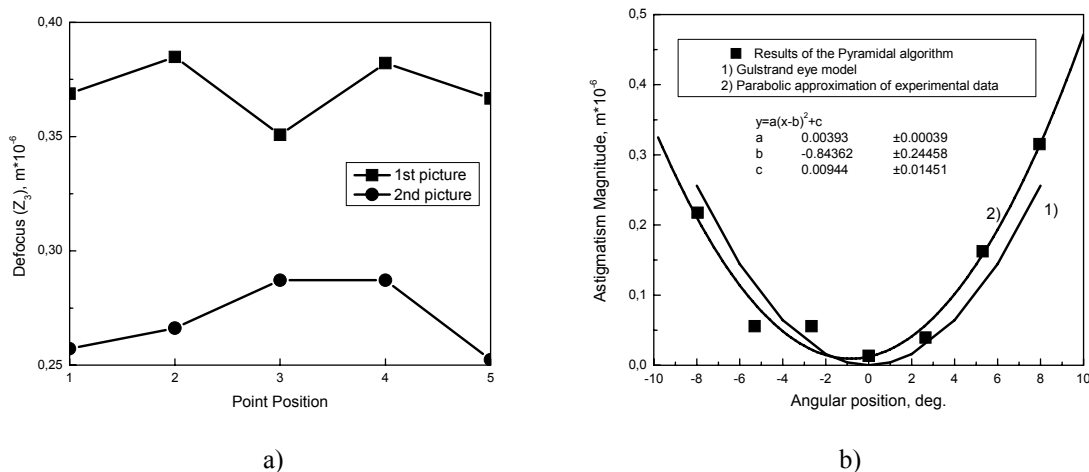


Figure 7. Defocus a) and astigmatism b) magnitudes, found for different positions on the retina.

order to let the algorithm work convergently. Results for two images, taken with different focal adjustment, are shown. From Fig.7 b) it is obvious that the dependence of astigmatism is in a good agreement with calculated theoretically from the Gullstrand model.

## CONCLUSION

An adaptive optical system, based on standard fundus imager and redesigned for using with a Shack-Hartmann wavefront sensor and a flexible mirror is capable of real-time tracking and suppressing aberrations of living eye. The angular field of view is limited by anisoplanatic errors and typically is about 4°. The angular behavior of aberrations is close to the model prediction. Deconvolution can increase the field of view of the system.

## ACKNOWLEDGMENT

This work is being funded by RFBR Grant 04-02-08114. The design of multi-layer coatings for the optical elements has been done with the help of OpiLayer software, provided by Research computer center of Moscow State University

## REFERENCES

1. Liang J., Grimm B., Goelz S., Bille J.F. "Objective measurement of wave aberrations of the human eye with use of a Hartmann-Shack wave-front sensor", *Opt. Soc. Am. A*, 11, 1949 (1994).
2. Liang J., Williams D.R., Miller D.T. "Supernormal vision and high-resolution retinal imaging through adaptive optics" *Opt. Soc. Am. A*, 14, 2884 (1997).
3. A.V. Larichev, P.V. Ivanov, N.G. Iroshnikov, V.I. Shmalhauzen, L.J. Otten "Adaptive system for eye-fundus imaging", *Quantum Electronics* 32(10) 902-908 (2002)
4. G. R. G. Erry, L. J. Otten, A. Larichev, N. Iroshnikov, "A high resolution adaptive optics fundus imager", 4<sup>th</sup> International Workshop on Adaptive Optics for Industry and Medicine, Muenster, Germany, October 19 - 24, 2003, Abstracts, p. 19, *Springer Proceedings in Physics*, p.333-341.
5. Larichev A.V., Iaitskova N.A., Shmalhausen V.I., "Field of view widening in non-astronomical adaptive systems", in *Adaptive Optics for Industry and Medicine*, Gordon D. Love ed., proc. the 2<sup>nd</sup> International Workshop on Adaptive Optics for Industry and Medicine, Durham, England (1999) pp.272-277.
6. Ignacio Iglesias. "Parametric wave-aberration retrieval from point-spread function data by use of a pyramidal recursive algorithm". *Applied Optics*, Vol. 37, No. 23, 10 August 1998.
7. Urmakher L.S., Aizenshtat L.I. *Oftal'mologicheskie pribory (Ophthalmologic Instruments)* (Moscow: Meditsina, 1988).

8. Tamarova R.M. *Opticheskie pribory dlya issledovaniya glaza (Optical Devices for Examination of Eye)* (Moscow: Meditsina, 1982).
9. Larichev A., Irochnikov N., Ivanov P., Kudryashov A. "Deconvolution of color retinal images with wavefront sensing", *Proc. SPIE Int. Soc. Opt. Eng.*, 4251, 102 (2001).
10. Larichev A.V., Ivanov P.V., Iroshnikov N.G., Shmalhauzen V.I., "Measurement of eye aberrations in a speckle field" *Kvantovaya Elektron.*, 31, 1108 (2001) [*Quantum Electron.*, 31, 1108 (2001)].
11. Delori F.C., Pflibsen K.P. "Spectral reflectance of the human ocular fundus" *Appl. Opt.*, 28, 1061 (1989).
12. Diaz Santana Haro L., Dainty J.C. "Single-pass measurements of the wave-front aberrations of the human eye by use of retinal lipofuscin autofluorescence", *Opt. Lett.*, 24, 61 (1999).
13. American National Standard for the Safe Use of Lasers, ANSI Z136.1 (Orlando, Fla., Laser Institute of America, 1993).
14. Normy i pravila ustroystva i ekspluatatsii lazerov (Norms and Regulations for Laser Arrangement and Operation) No. 5804-91 (Moscow, 1991).
15. Southwell W.H., "Wavefront estimation from wavefront slope measurements,". *Opt. Soc. Am.*, 70, 998 (1980).
16. Born M., Wolf E. *Principles of Optics*, Oxford: Pergamon Press, 1969.
17. Fried D., "Anisoplanatism in adaptive optics", *Opt. Soc. Am. A*, 72, 52 (1982).
18. Johnston D., Welsh B. "Analysis of multiconjugate adaptive optics" *Opt. Soc. Am. A*, 11, 394 (1994).
19. James N. Caron, Nader M. Namazi, and Chris J. Rollins. "Noniterative blind data restoration by use of an extracted filter function". *Applied Optics*, Vol. 41, No. 32, 10 November 2002.
20. Nelder, J.A. and Mead, R., "A Simplex Method for Function Minimization", *Computer Journal*, Vol. 7, Issue 4 (1965), 308-313.